Growth of Well Aligned IrO_2 Nanotubes on $LiTaO_3$(012) Substrate

Reui-San Chen,[†] Ying-Sheng Huang,*[,†] Dah-Shyang Tsai,[‡] Surajit Chattopadhyay,[§] Chien-Ting Wu,[§] Zon-Huang Lan,[§] and Kuei-Hsien Chen[§]

Department of Electronic Engineering, National Taiwan University of Science and Technology, Taipei 106, Taiwan, Department of Chemical Engineering, National Taiwan University of Science and Technology, Taipei 106, Taiwan, and Institute of Atomic and Molecular Sciences, Academia Sinica, Taipei 106, Taiwan

Received November 24, 2003. Revised Manuscript Received March 30, 2004

Self-assembled and well-aligned IrO_2 nanotubes have been grown on $LiTaO_3$ (LTO) (012) substrates via metal-organic chemical vapor deposition (MOCVD), using (methylcyclopentadienyl)(1,5-cyclooctadiene)iridium(I) as the source reagent. The surface morphology, structural, and spectroscopic properties of the as-deposited nanotubes were characterized using field-emission scanning electron microscopy (FESEM), transmission electron microscopy (TEM), X-ray diffraction (XRD), and micro-Raman spectroscopy. FESEM and TEM micrographs revealed that the single-crystalline nanotubes were grown with a tilt angle of ∼35° from the normal to the substrate. The IrO_2 nanotubes showed square cross-sections and open-end morphology with the long axis toward the [001] direction. The analysis of selected area diffraction (SAD) and XRD patterns indicated the epitaxial growth of IrO_2 nanotubes on LTO (012) with the orientation relationship given by IrO_2(101)//LTO(012) and $IrO_2[0\bar{1}0]$//LTO[100]. The probable mechanism for the formation of nanotubes has been discussed. Micro-Raman spectrum shows the red-shift and peak broadening of the IrO_2 signatures with respect to that of the bulk counterpart which may be indicative of a phonon confinement effect for these nanotubes.

Introduction

The discovery of carbon nanotubes (CNT)[1] caused an avalanche in nanoscale research with perennial efforts to uncover new nanostructures of single elements and compounds. This saw the evolution of metallic, polymeric, and more importantly semiconducting nanostructures, including CNT analogues (BN,[2] BC,[3] and $B_xC_yN_z$[4]), layered chalcogenides (WS_2,[5] ReS_2,[6] MoS_2,[7] NbS_2, TaS_2,[8] $MoSe_2$, and WSe_2[9]), etc. One-dimensional (1D) nanoscaled materials, such as nanowires, nanorods, and nanotubes, proved to be an ideal system to study the effect of low dimensionality on their physical and chemical properties, which remain as critical functions of their dimensions and surface structures. The huge surface area of these one-dimensional nanostructures, that play an important role in governing their properties, is also the root cause for their degradation and instability. However the wide band gap and oxide nanostructures such as SiCN nanorods[10] or ZnO nanobelts[11] are comparatively stable. This fact has led researchers to apply an overcoat of stable boron nitride[12] or silica[13] on the otherwise unstable nanostructures. The important applications of oxides have also brought out significant efforts for the synthesis of certain oxide nanotubes, such as VO_x,[14] TiO_2,[15] ZnO,[16] ZrO_2,[17] SiO_2, Al_2O_3,[18] In_2O_3,[19] $W_{18}O_{49}$,[20] and rare-earth oxides.[21]

* Corresponding author. E-mail: ysh@et.ntust.edu.tw.
[†] Department of Electronic Engineering, National Taiwan University of Science and Technology.
[‡] Department of Chemical Engineering, National Taiwan University of Science and Technology.
[§] Institute of Atomic and Molecular Sciences, Academia Sinica.

(1) Ijima, S. *Nature* **1991**, *354*, 56.
(2) Chopra, N. G.; Luyken, R. J.; Cherrey, K.; Crespi, V. H.; Cohen, M. L.; Louie, S. G.; Zettl, A. *Science* **1995**, *269*, 966. Han, W.; Bando, Y.; Kurashima, K.; Sato, T. *Appl. Phys. Lett.* **1998**, *73*, 3085. Golberg, D.; Han, W.; Bando, Y.; Bourgeois, L.; Kurashima, K.; Sato, T. *Appl. Phys. Lett.* **1999**, *86*, 2364. Bengu, E.; Marks, L. D. *Phys. Rev. Lett.* **2001**, *86*, 2385.
(3) Satishkumar, B. C.; Govindaraj, A.; Harikumar, K. R.; Zhang, J. P.; Cheetham, A. K.; Rao, C. N. R. *Chem. Phys. Lett.* **1999**, *300*, 473.
(4) Stephan, O.; Ajayan, P. M.; Colliex, C.; Ph. Redlich; Lambert, J. M.; Bernier, P.; Lefin, P. *Science* **1994**, *266*, 1683.
(5) Tenne, R.; Margulis, L.; Genut, M.; Hodes, G. *Nature* **1992**, *360*, 444.
(6) Brorson, M.; Hansen, T. W.; Jacobsen, C. J. H. *J. Am. Chem. Soc.* **2002**, *124*, 11582.
(7) Feldman, Y.; Wasserman, E.; Srolovitz, D. J.; Tenne, R. *Science* **1995**, *267*, 222. Remskar, M.; Mrzel, A.; Skraba, Z.; Jesih, A.; Ceh, M.; Demsar, J.; Stadelmann, P.; Levy, F.; Mihailovic, D. *Science* **2001**, *292*, 479.
(8) Nath, M.; Rao, C. N. R. *J. Am. Chem. Soc.* **2001**, *123*, 4841.
(9) Nath, M.; Rao, C. N. R. *Chem. Commun.* **2001**, 2236.
(10) Chen, L. C.; Chang, S. W.; Chang, C. S.; Wen, C. Y.; Wu, J. J.; Chen, Y. F.; Huang, Y. S.; Chen, K. H. *J. Phys. Chem. Solids* **2001**, *62*, 1567.
(11) Pan, Z. W.; Dai, Z. R.; Wang, Z. L. *Science* **2001**, *291*, 1947.
(12) Yi, W.; Jeong, T.; Yu, S.; Heo, J.; Lee, C.; Lee, J.; Kim, W.; Yoo, J. B.; Kim, J. *Adv. Mater.* **2002**, *14*, 1464.
(13) Whitsitt, E. A.; Barron, A. R. *Nano Lett.* **2003**, *3*, 775.
(14) Spahr, M. E.; Bitterli, P.; Nesper, R.; Muller, M.; Krumeich, F.; Nissen, H. U. *Angew. Chem., Int. Ed. Engl.* **1998**, *37*, 1263. Muhr, H. J.; Krumeich, F.; Schonholzer, U. P.; Bieri, F.; Niederberger, M.; Gauckler, L. J.; Nesper, R. *Adv. Mater.* **2000**, *12*, 231. Krumeich, F.; Muhr, H. J.; Niederberger, M.; Bieri, F.; Schnyder, B.; Nesper, R. *J. Am. Chem. Soc.* **1999**, *121*, 8324.

10.1021/cm030668n CCC: $27.50
Published on Web 05/07/2004

Conductive IrO_2 exhibits high thermal and chemical stability, making their films valuable as durable electrodes in electrochemical and microelectronic devices.[22] In recent reports, IrO_2 has also been studied as a high performance and robust field emitter owing to its low work function, low resistivity, and excellent stability against oxygen.[23]

The synthesis of IrO_2 nanorods has been previously reported via the template-based method.[24] For practical applications, we have developed a simpler method to fabricate large area and high-density IrO_2 nanorods on Si[25] and metal-coated-Si wafers[26] by metal-organic chemical vapor deposition (MOCVD). The 1D growth behavior of IrO_2 is found to be highly correlated to both the oxygen-rich ambient and growth temperature instead of the catalyst.[25,26] In the present work, we rely on a similar CVD approach and control the deposition rate to epitaxially grow self-assembled and well aligned IrO_2 nanotubes on a $LiTaO_3$ (LTO) (012) substrate. The surface morphology, structural, and spectroscopic properties of the as-deposited nanotubes were examined by using field-emission scanning electron microscopy (FESEM), transmission electron microscopy (TEM), X-ray diffraction (XRD), and micro-Raman spectroscopy. A strong substrate effect on the alignment of the IrO_2 nanotube growth is observed, and the probable mechanism for the formation of the nanotubes is discussed.

Experimental Section

The CVD experiments were carried out in a vertical-flow cold-wall reactor using the low-melting iridium source reagent (methylcyclopentadienyl)(1,5-cyclooctadiene)iridium(I) supplied by Strem Chemicals. The $LiTaO_3$ (012) wafer was used as the substrate for aligned growth of IrO_2 nanotubes. Both the precursor reservoir and the transport line were controlled in the temperature range of 90−110 °C to avoid precursor condensation during the vapor-phase transport. High purity oxygen, flow rate 100 sccm, was used as the carrier gas. During the deposition, the substrate temperature was kept at 350 °C, and the chamber pressure was held within the range of 20−50 Torr to obtain the IrO_2 1D crystals. The deposition rate of the 1D crystals with tubular morphology was estimated to be 5−10 nm/min. The deposition rate was also adjusted, by varying the partial pressure of iridium precursor, to study the kinetic factors involved in growing the 1D crystals.

The micrographs and the stoichiometry of the IrO_2 nanotubes were determined by a JEOL-JSM6500F FESEM instrument. TEM images and electron diffraction patterns were recorded to check the preferential growth direction of individual IrO_2 nanotubes (JEOL 2010F FEG TEM). XRD patterns recorded on a Rigaku RTP300RC spectrometer were used to examine the growth orientation over a large area. Raman scattering spectroscopy was used to extract microstructural information about the IrO_2 nanotubes by using a Jobin-YvonT64000 micro-Raman system, equipped with an Ar-ion laser having an excitation wavelength 514.5 nm which was focused on the sample using an optical microscope.

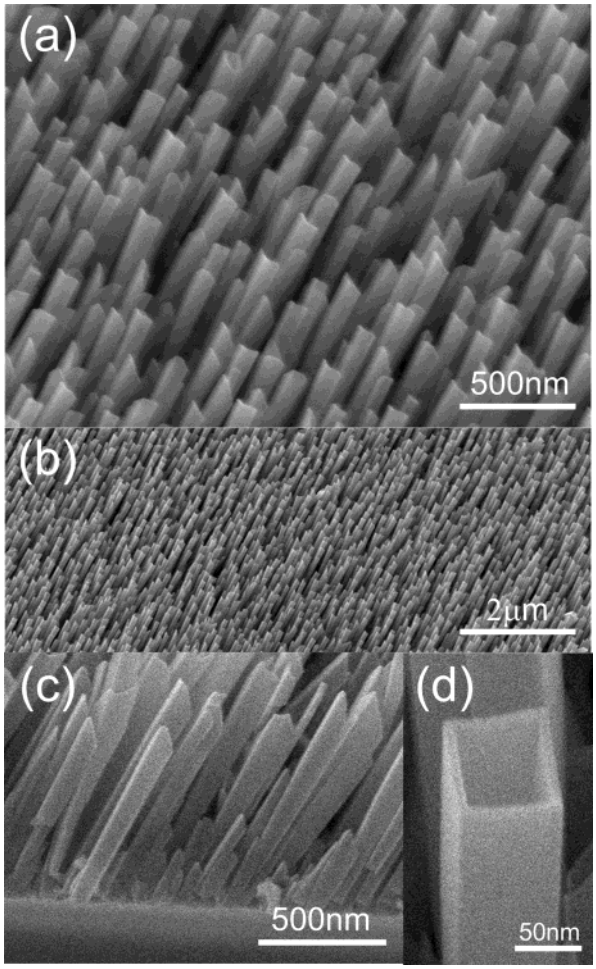

Figure 1. FESEM images of the well aligned IrO_2 nanotubes grown on $LiTaO_3$ (012) substrate: (a) and (b) top view; (c) cross view; (d) focus on a typical IrO_2 nanotube.

Results and Discussion

As illustrated in Figure 1, the FESEM images show high density and well aligned IrO_2 nanotubes grown on a LTO (012) substrate. The self-assembled nanotubes

(15) Kasuga, T.; Hiramatsu, M.; Hoson, A.; Sekino, T.; Niihara, K. *Langmuir* **1998**, *14*, 3160. Imai, H.; Takei, Y.; Shimizu, K.; Matsuda, M.; Hirashima, H. *J. Mater. Chem.* **1999**, *9*, 2971. Kasuga, T.; Hiramatsu, M.; Hoson, A.; Sekino, T.; Niihara, K. *Adv. Mater.* **1999**, *11*, 1307. Kobayashi, S.; Hanabusa, K.; Hamasaki, N.; Kimura, M.; Shirai, H. *Chem. Mater.* **2000**, *12*, 1523. Du, G. H.; Chen, Q.; Che, R. C.; Yuan, Z. Y.; Peng, L. M. *Appl. Phys. Lett.* **2001**, *79*, 3702. Gong, D.; Grimes, C. A.; Varghese, O. K.; Hu, W.; Singh, R. S.; Chen, Z.; Dickey, E. C. *J. Mater. Res.* **2001**, *16*, 3331. Caruso, R. A.; Schattka, J. H.; Greiner, A. *Adv. Mater.* **2001**, *13*, 1577. Liu, S. M.; Gan, L. M.; Liu, L. H.; Zhang, W. D.; Zeng, H. C. *Chem. Mater.* **2002**, *14*, 1391.

(16) Vayssieres, L.; Keis, K.; Hagfeldt, A.; Lindquist, S. E. *Chem. Mater.* **2001**, *13*, 4395.

(17) Rao, C. N. R.; Satishkumar, B. C.; Govindaraj, A. *Chem. Commun.* **1997**, 1581.

(18) Satishkumar, B. C.; Govindaraj, A.; Vogl, E. M.; Basumallick, L.; Rao, C. N. R. *J. Mater. Res.* **1997**, *12*, 604.

(19) Li, Y.; Bando, Y.; Golberg, D. *Adv. Mater.* **2003**, *15*, 581.

(20) Li, Y.; Bando, Y.; Golberg, D. *Adv. Mater.* **2003**, *15*, 1294.

(21) Wang, X.; Sun, X.; Yu, D.; Zou, B.; Li, Y. *Adv. Mater.* **2003**, *15*, 1442.

(22) Cogan, S. F.; Plante, T. D.; McFadden, R. S.; Rauh, R. D. *Sol. Energy Mater.* **1987**, *16*, 371. Nakamura, T.; Nakao, Y.; Kamisawa, A.; Takasu, H. *Appl. Phys. Lett.* **1994**, *65*, 1522. Lee, H. S.; Um, W. S.; Hwang, K. T.; Shin, H. G.; Kim, Y. B.; Auh, K. H. *J. Vac. Sci. Technol. A* **1999**, *17*, 2939. Song, Y. J.; Kim, H. H.; Lee, S. Y.; Jung, D. J.; Koo, B. J.; Lee, J. K.; Park, Y. S.; Cho, H. J.; Park, S. O.; Kim, K. *Appl. Phys. Lett.* **2000**, *76*, 451. Shin, J. C.; Hwang, C. S.; Kim, H. J. *Appl. Phys. Lett.* **2000**, *76*, 1609. Pinnow, C. U.; Kasko, I.; Nagel, N.; Poppa, S.; Mikolajick, T.; Dehm, C.; Hosler, W.; Bleyl, F.; Jahnel, F.; Seibt, M.; Geyer, U.; Samwer, K. *J. Appl. Phys.* **2002**, *91*, 9591.

(23) Chalamala, B. R.; Wallace, R. M.; Gnade, B. E. *J. Vac. Sci. Technol. B* **1998**, *16*, 2859. Chalamala, B. R.; Wei, Y., Reuss, R. H.; Aggarwal, S.; Gnade, B. E.; Ramesh, R.; Bernhard, J. M.; Sosa, E. D.; Golden, D. E. *Appl. Phys. Lett.* **1999**, *74*, 1394. Chalamala, B. R.; Reuss, R. H.; Dean, K. A.; Sosa, E.; Golden, D. E. *J. Appl. Phys.* **2002**, *91*, 6141. Chen, R. S.; Huang, Y. S.; Liang, Y. M.; Hsieh, C. S.; Tsai, D. S.; Tiong, K. K. *Appl. Phys. Lett.* **2004**, *84*, 1552.

(24) Satishkumar, B. C.; Govindaraj, A.; Nach, M.; Rao, C. N. R. *J. Mater. Chem.* **2000**, *10*, 2115.

(25) Chen, R. S.; Chen, Y. S.; Huang, Y. S.; Chen, Y. L.; Chi, Y.; Liu, C. S.; Tiong, K. K.; Carty, A. J. *Chem. Vap. Deposition* **2003**, *9*, 301.

(26) Chen, R. S.; Huang, Y. S.; Liang, Y. M.; Tsai, D. S.; Chi, Y.; Kai, J. J. *J. Mater. Chem.* **2003**, *13*, 2525.

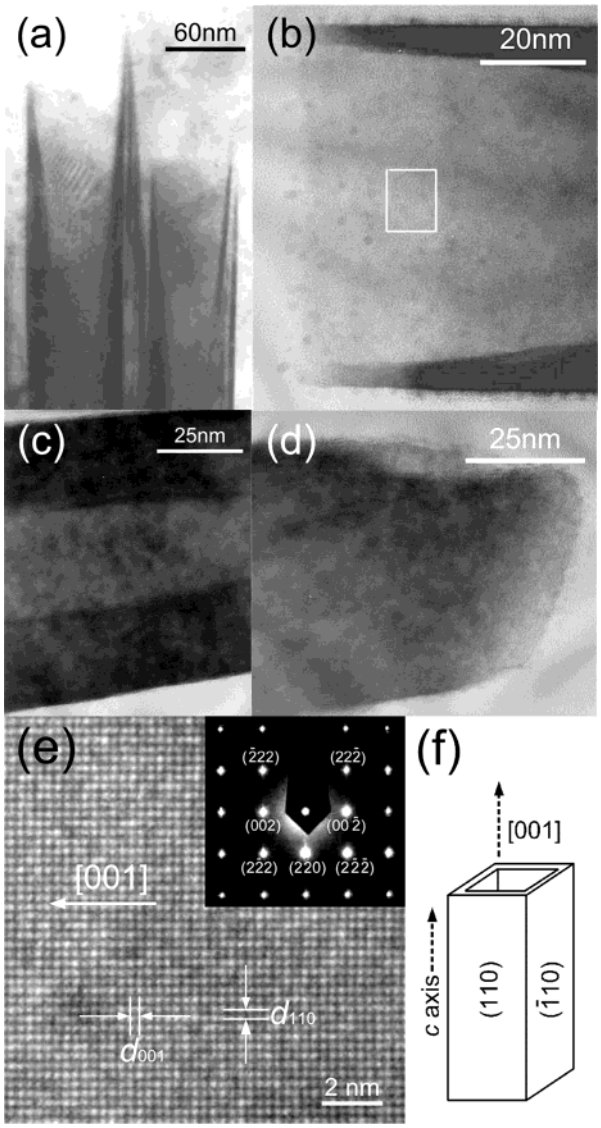

Figure 2. TEM images of the IrO_2 nanotubes focused on (a) two individual tubes; (b) the front end; (c) the middle; (d) the bottom. (e) The high-resolution TEM image and its SAD pattern taken from the tube-wall in 2(b). (f) A schematic diagram of the IrO_2 nanotube.

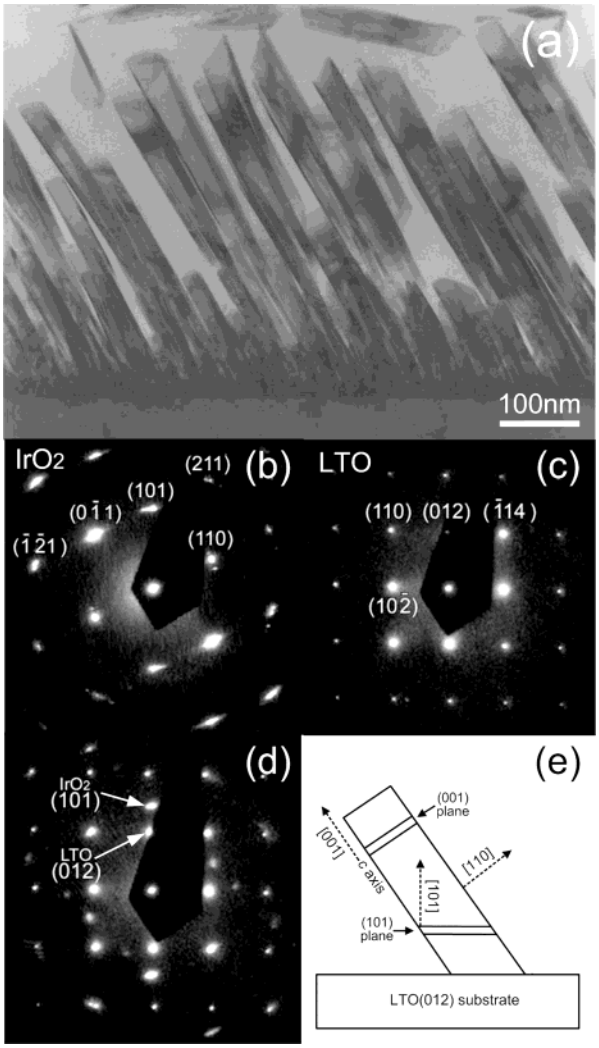

Figure 3. (a) The cross-sectional TEM image of the IrO_2 nanotubes on $LiTaO_3$ (012) substrate and its corresponding SAD patterns taken separately from the regions of (b) IrO_2 nanotubes, (c) $LiTaO_3$ substrate, and (d) interface along the zone axes of IrO_2 [$\bar{1}$11] and $LiTaO_3$ [2$\bar{2}$1]. (e) The schematic diagram of the orientation relationship between the nanotube and substrate.

were grown with an identical tilt angle from the normal to the substrate. Unlike the cylindrical symmetry of most of the nanotubes reported so far, the IrO_2 tubes show open ends with a square cross-section. The estimated edge size, length, and packing density are 50−80 nm, 1.0−1.5 μm, and 75 ± 5 μm^{-2}, respectively. Energy-dispersive X-ray spectroscopy (EDS) measurements indicate that the tubules have an average atomic ratio of Ir to O of 1:2.

The TEM images, depicted in Figure 2a−d, show the tubular morphology of the IrO_2 nanocrystals. TEM images focused on the front end, middle, and bottom end of the nanotube are depicted in parts b−d of Figure 2, respectively, showing the nonuniform tube wall thickness, which tends to decrease from the bottom to the open-end. As shown in Figure 2e, a high-resolution TEM image taken from the tube wall marked in Figure 2b exhibits clear lattice planes of the IrO_2 nanotube, and the lattice spacing between adjacent lattice planes for both the (001) and (110) planes is about 0.31 nm. The corresponding selected area diffraction (SAD) pattern (inset, Figure 2e) is identified to be the [110] zone pattern, indicating that the tube walls belong to the {110} facets and the preferential growth direction of the IrO_2 tubes is along the [001] direction (*c* axis). A schematic of the tubular crystal of IrO_2 is illustrated in Figure 2f. The results also confirm the tetragonal rutile structure and single crystalline quality of the IrO_2 nanotubes.

The cross-sectional TEM image in Figure 3a shows that all of the IrO_2 nanotubes grow with a tilt angle of ∼35° from the normal to the substrate surface. By separately focusing on the nanotubes and substrate, the tetragonal IrO_2 [$\bar{1}$11] and rhombohedral LTO [2$\bar{2}$1] zone patterns are obtained and shown in parts b and c of Figure 3, respectively. Furthermore, a mixed SAD pattern at the interface region, depicted in Figure 3d, indicates that the IrO_2 (101) layers are heteroepitaxially deposited on the LTO (012) substrate. This result is further confirmed by XRD measurements. Figure 4 shows a typical XRD pattern of the well aligned IrO_2 nanotubes grown on LTO (012) substrate. Two peaks at around 35° and 73° are indexed as (101) and (202),

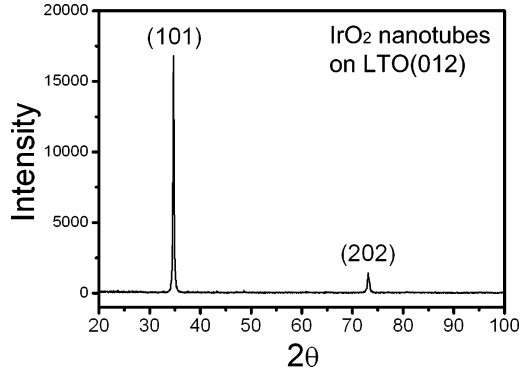

Figure 4. The typical XRD pattern of the well aligned IrO_2 nanotubes grown on $LiTaO_3$ (012) substrate.

respectively, of rutile IrO_2, indicating that all the IrO_2 (101) planes are parallel to the substrate plane. In addition, these results also provide a reasonable explanation of the substrate effect on the tilted growth of the IrO_2 nanotubes. Initially, the deposition of IrO_2 starts from the epitaxy of the {101} planes on the LTO (012) surface. Since the long axis of nanotube is along the [001] direction, the growth rate of (00*l*) planes should be the highest in this case. Then the tilted growth occurs along the [001] direction which is 35.04° from the normal to the LTO (012) substrate or IrO_2 (101) plane. Figure 3e illustrates the schematic diagram of the orientation relationship between IrO_2 nanotubes and the LTO substrate.

Moreover, the orientation relationship can be explained based on the lattice misfits present between the IrO_2 and LTO substrate. The lattice misfit at the interface produces strain energy when the IrO_2 is nucleated. The orientation that minimizes the lattice misfit and produces the smallest strain energy will be preferred. A schematic drawing of the epitaxial relationship of IrO_2 and LTO is depicted in Figure 5. This growth pattern results in the smallest lattice mismatches between the IrO_2 nanotubes and the substrate, in which the lattice spacing along IrO_2 $[\bar{1}01]$ (0.54941 nm) nearly matches with the LTO $[\bar{1}\bar{2}1]$ (0.54682 nm), while the IrO_2 $[0\bar{1}0]$ along the LTO [100] shows a mismatch of ~12.7%, where the lattice parameters are $a = b = 0.44983$ nm and $c = 0.31544$ nm for IrO_2[27] and $a = b = 0.51530$ nm and $c = 1.3755$ nm for LTO.[28] Therefore the overall orientation relationship between the IrO_2 and LTO can be described as IrO_2 (101)//LTO (012) and IrO_2 $[0\bar{1}0]$//LTO [100].

Our earlier studies have indicated that the stable dioxide phase is preferentially formed under the combination of higher substrate temperatures (≥350 °C) and higher oxygen ambient pressures (≥10 Torr). Depositions at lower temperatures (≤300 °C) or lower pressures (≤1 Torr) would result in the predominant Ir metal phase.[25] In particular, 1D growth habit for the IrO_2 crystals was found under more specific conditions (300−350 °C and 30 Torr).[25] The strong substrate effect on the alignment of the IrO_2 nanotubes during growth has been shown, where the tilted alignment of the IrO_2 tubes can be understood by the lattice misfits at the

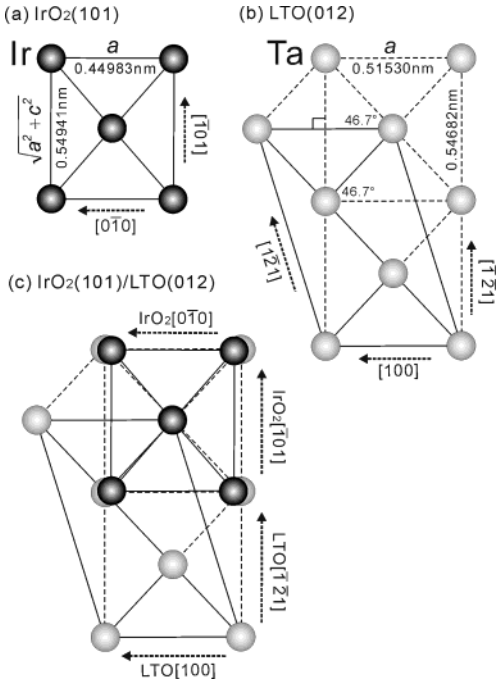

Figure 5. The schematic drawing of the epitaxial relationship between IrO_2 and $LiTaO_3$: (a) IrO_2 (101) plane; (b) $LiTaO_3$ (012) plane; (c) epitaxy of IrO_2 (101)/$LiTaO_3$ (012).

interface. However, the upward growth of a tube from the interface with the morphology of a square cross-section with an open end is another question of scientific interest. We shall discuss the origin of this tube morphology in terms of two aspects: the *c*-axis directional growth and the spiral growth in the plane perpendicular to the *c*-axis.

Directional growth of IrO_2 in the *c*-axis is always observed regardless of whether a wedge-shaped rod (see Figure 6a) or a square tube is formed (Figure 6c).[26] The [001] growth direction is preferred since the (002) plane is the least stable among (110), (101), and (002) planes. In addition, the {110} planes are the most stable crystal planes for rutile structure materials.[29] Thus the IrO_2 growth proceeds to eliminate the (002) planes via forming its perpendicular {110} planes, accordingly the crystal elongates in the [001] direction with a square geometry.

The above remarks do not explain why IrO_2 grows into a tube and a wedge-shaped rod, instead of a solid square rod. A plausible explanation is that IrO_2 grows in a spiral mode on the plane perpendicular to the [001] direction. We observe such a spiral growth at the rod tops occasionally (Figure 7).[26] Although the reason behind the spiral growth mode of IrO_2 is not clear at this stage, nevertheless a spiral growth in conjunction with a *c*-axis growth provides a way of forming a hollow tube-shape crystal.

We can demonstrate the connection between a square tube and a wedge-shape rod of IrO_2 by changing the deposition rate. The deposition rate is varied by increasing the partial pressure of the iridium precursor in the CVD chamber. The influence of an increasing deposition rate is illustrated in Figure 6. The IrO_2 nanotubes are grown when the deposition rate is slow 5−10 nm/min,

(27) JCPDS card no. 15-0870, International Centre for Diffraction Data, Newtown Square, PA.

(28) JCPDS card no. 29-0836, International Centre for Diffraction Data, Newtown Square, PA.

(29) Vetrone, J.; Foster, C. M.; Bai, G. R.; Wang, A.; Patel, J.; Wu, X *J. Mater. Res.* **1998**, *13*, 2281.

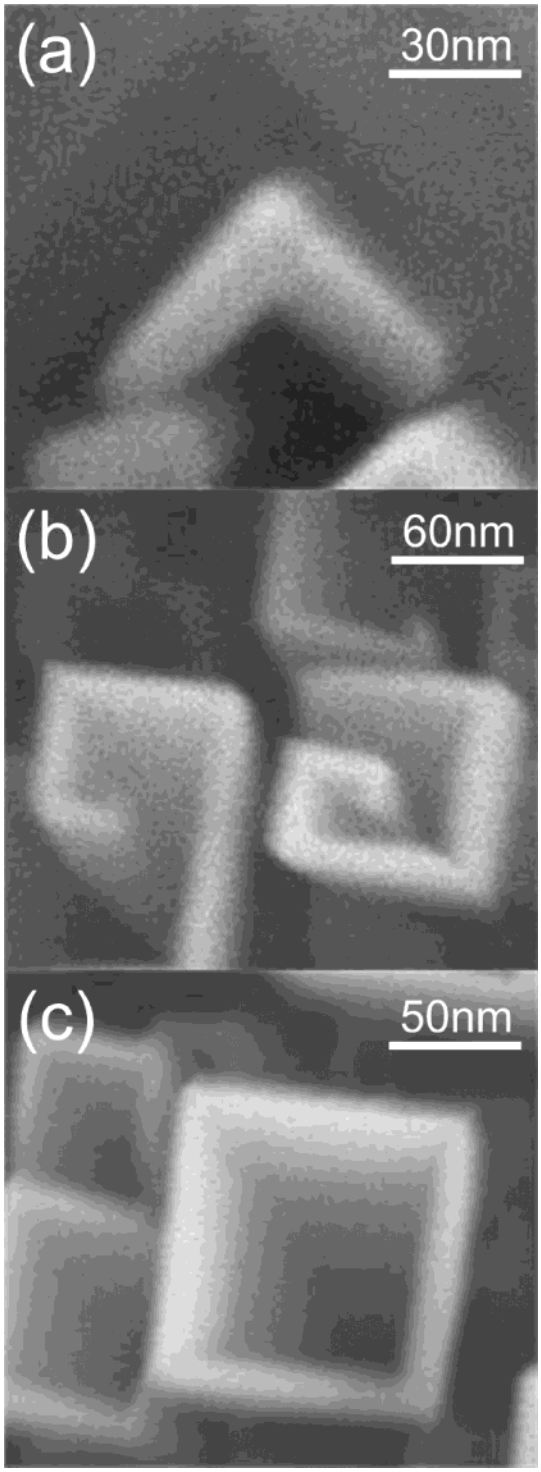

Figure 6. IrO_2 1D geometry variation owing to the increase in deposition rate: (a) a tube, (b) an improperly enclosed tubular geometry, (c) a wedge-shaped rod.[26]

Figure 6c. Increasing the deposition rate to 12−18 nm/min results in a number of improperly enclosed tubes, Figure 6b. When the deposition rate was further increased to over 20 nm/min, nanorods with wedge shape are grown, Figure 6a.[26] It seems that a square tube will form when the depositing atoms have sufficient time to complete the square loop via the spiral growth mode. When the deposition atoms have insufficient time, 1D structures of lower symmetry are formed instead.

The micro-Raman spectroscopy was used to extract microstructural information about the IrO_2 nanotubes.

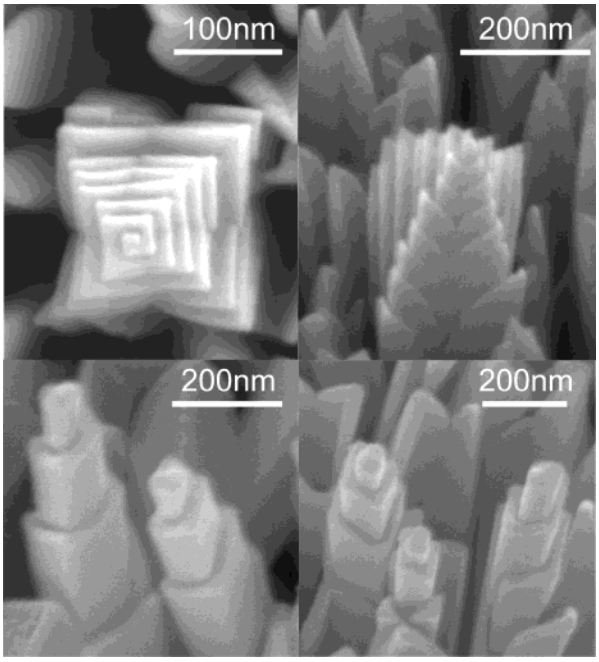

Figure 7. The FESEM images of the IrO_2 nanocrystal exhibiting spiral growth behavior.[26]

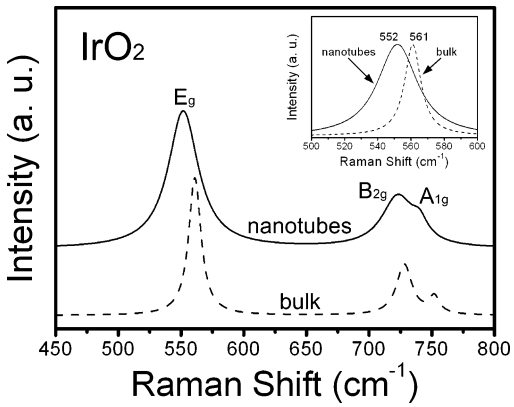

Figure 8. The micro-Raman spectra of the IrO_2 nanotubes and the bulk material.

Figure 8 shows the Raman spectra of the IrO_2 nanotubes (solid line) and its bulk material (dashed line) in the range of 450−800 cm^{-1}, in which three Raman modes, identified as E_g, B_{2g}, and A_{1g} were observed. By analyzing the main scattering signal of the E_g mode (see the inset, Figure 8), the nanotubes exhibit a 9 cm^{-1} red-shift in peak position (E_g at 552 cm^{-1}) and broader line width (full width at half-maximum; fwhm ∼28 cm^{-1}) as compared with the bulk (E_g at 561 cm^{-1}, fwhm = 12 cm^{-1}).[30] The 9 cm^{-1} red-shift in peak position and broadening of the line shape of the IrO_2 nanotubes may be attributed to the nanoscale nature of the oxide tubules. Red-shifts in the Raman peak positions for IrO_2 thin films relative to those of single-crystalline IrO_2 are well-known, with a broadening of the peaks as the films become less ordered.[30] The strain and disorder in the lattice could result in the peak shift as well. However, the strain effect is restricted to the interface region and should be minimal for the other parts of the 1D

(30) Huang, Y. S.; Lin, S. S.; Huang, C. R.; Lee, M. C.; Dann, T. E.; Chien, F. Z. *Solid State Commun.* **1989**, *70*, 517. Liao, P. C.; Chen, C. S.; Ho, W. S.; Huang, Y. S.; Tiong, K. K. *Thin Solid Films* **1997**, *301*, 7.

materials such as nanotubes or nanowires having the least contact area with substrate. The formation of IrO_2 nanotubes of single crystalline quality, as determined from the TEM and XRD studies, also rules out the possibility of significant disorder in the structure. Accordingly, the result of the peak shift and line broadening may be more related to the nanoscale nature of the 1D oxide materials,[31] and possible phonon confinement effects cannot be ruled out.[32]

Conclusions

High density and well-aligned IrO_2 nanotubes have been grown on LTO (012) substrates via the MOCVD technique. Using the SEM, TEM, SAD, and XRD analyses, the single-crystalline nanotubes were shown to grow with a tilt angle of ~35° from the normal to the substrate. The IrO_2 nanotubes showed square cross-sections and an open-end morphology with the long axis toward the [001] direction. The initial IrO_2 (101) epitaxial nucleation on the LTO (012) surface was found to be the key factor in the tilted growth of the nanotubes. The formation of the IrO_2 nanotubes might be attributed to the spiral growth in the plane perpendicular to the *c*-axis under a slower deposition rate. The micro-Raman spectrum shows a red-shift and peak broadening of the IrO_2 signatures with respect to that of the bulk counterpart which may be indicative of a phonon confinement effect for these nanotubes. These results could be useful in providing a new direction to the growth control of 1D nanostructures.

Acknowledgment. The authors wish to acknowledge the support of the National Science Council of Taiwan.

CM030668N

(31) Ryan, J. V.; Berry, A. D.; Anderson, M. L.; Long, J. W.; Stroud, R. M.; Cepak, V. M.; Browning, V. M.; Rolison, D. R.; Merzbacher, C. I. *Nature* **2000**, *406*, 169. Rajalakshmi, M.; Arora, A. K.; Bendre, B. S.; Mahamuni, S. *J. Appl. Phys.* **2000**, *87*, 2445. Kosacki, I.; Petrovsky, V.; Anderson, H. U.; Colomban, P. *J. Am. Ceram. Soc.* **2002**, *85*, 2646. Kosacki, I.; Suzuki, T. H.; Anderson, U.; Colomban, P. *Solid State Ionics* **2002**, *149*, 99.

(32) Parayanthal, P.; Pollak, F. H. *Phys. Rev. Lett.* **1984**, *52*, 1822. Liu, H. L.; Chen, C. C.; Chia, C. T.; Yeh, C. C.; Chen, C. H.; Yu, M. Y.; Keller, S.; DenBaars, S. P. *Chem. Phys. Lett.* **2001**, *345*, 245.